PAPER

Single atom devices by ion implantation

IOP Publishing Journal of Physics: Condensed Matter
J. Phys.: Condens. Matter **27** (2015) 154204 (9pp) doi:10.1088/0953-8984/27/15/154204

Single atom devices by ion implantation

Jessica van Donkelaar[1], C Yang[1], A D C Alves[1,3], J C McCallum[1], C Hougaard[1], B C Johnson[1], F E Hudson[2], A S Dzurak[2], A Morello[2], D Spemann[1] and D N Jamieson[1]

[1] Centre for Quantum Computation and Communication Technology, School of Physics, University of Melbourne, Melbourne, Victoria 3010, Australia
[2] Centre for Quantum Computation and Communication Technology, School of Electrical Engineering and Telecommunications, UNSW Australia, Sydney, New South Wales 2052, Australia

E-mail: d.jamieson@unimelb.edu.au

Received 21 August 2014, revised 20 November 2014
Accepted for publication 2 December 2014
Published 18 March 2015

Abstract

To expand the capabilities of semiconductor devices for new functions exploiting the quantum states of single donors or other impurity atoms requires a deterministic fabrication method. Ion implantation is a standard tool of the semiconductor industry and we have developed pathways to deterministic ion implantation to address this challenge. Although ion straggling limits the precision with which atoms can be positioned, for single atom devices it is possible to use post-implantation techniques to locate favourably placed atoms in devices for control and readout. However, large-scale devices will require improved precision. We examine here how the method of ion beam induced charge, already demonstrated for the deterministic ion implantation of 14 keV P donor atoms in silicon, can be used to implant a non-Poisson distribution of ions in silicon. Further, we demonstrate the method can be developed to higher precision by the incorporation of new deterministic ion implantation strategies that employ on-chip detectors with internal charge gain. In a silicon device we show a pulse height spectrum for 14 keV P ion impact that shows an internal gain of 3 that has the potential of allowing deterministic implantation of sub-14 keV P ions with reduced straggling.

Keywords: deterministic doping, ion implantation, ion beam induced charge, nanostencil

(Some figures may appear in colour only in the online journal)

1. Introduction

To address the challenge of the fabrication of devices which exploit the internal quantum degrees of freedom of single atoms in the solid state a number of techniques are being developed (Schofield *et al* 2003, Jamieson *et al* 2005, Shinada *et al* 2005, Batra *et al* 2007, Johnson *et al* 2010, Jacob *et al* 2014). These devices could incorporate quantum systems that bridge the foundations of modern information technology based on silicon into the future of ultra-scaled devices where quantum mechanics offers new functionalities for information sensing, storage, processing and transmission (Dowling and Milburn 2003).

Here we focus on the development of a technique that employs ion implantation that is compatible with the process flow for the fabrication of single atom semiconductor devices with the standard tools of the industry (Jamieson *et al* 2001). The implantation of swift ions into semiconductor materials has a long history (Wegmann 1980, Rose 1985, Gibbons 1987) and the semiconductor industry presently employs many implantation steps in the fabrication of a typical large-scale integrated circuit (Chason *et al* 1997, Poate and Saadatmand 2002). It is therefore attractive to employ this standard technique for our purposes. Some parameters for the near-surface ion implantation of donors into silicon and diamond are given in table 1. Although the focus of this paper is on the Si : P system, the data for diamond is included because considerable work has been done exploring the potential for ion implantation to fabricate colour centres in diamond for various quantum technologies. Some progress is being made on the deterministic conversion of implanted N ions into shallow N–V^- colour centres in diamond and activation as high as 37%

[3] Current address: Australian Radiation Protection and Nuclear Safety Agency, 619 Lower Plenty Road, Yallambie VIC 3085, Australia.

Table 1. Characteristics of implanted donors in Si and C. Bohr orbit data from Koiller *et al* (2006), implantation data from SRIM (Ziegler *et al* 2010).

Matrix : Donor	Bohr orbit diameter (nm)	Energy for 20 nm depth (keV)	Lateral straggling (nm)	Number of e–h pairs per impact
C(diamond) : N	—	15	6.3	710
Si : P	2.44	12	8.5	1400
Si : As	1.96	20	5.7	2100
Si : Sb	2.64	22	4.8	2250
Si : Bi	1.94	28	3.7	3100

has been reported (Naydenov *et al* 2010) for 300 keV implant energy and appropriate annealing although the conversion efficiency decreases to 5% for 20 keV implant energy or below (Toyli *et al* 2010, Schwartz *et al* 2011). Further improvement can be expected in the near future as understanding of the thermodynamics of this system increases.

Nanoscale devices based on Si : P with implanted, activated donors selected post-implantation by tuned gate potentials have shown that it is possible to control and readout the single ^{31}P donor electron spin (Morello *et al* 2010, Laucht *et al* 2014), measure the electron spin coherence in natural silicon (Pla *et al* 2012), ^{31}P nuclear spin in natural silicon (Pla *et al* 2013) and the electron and ^{31}P nuclear spins in isotopically enriched ^{28}Si (Muhonen *et al* 2014). Also some insights have been gained into the coupling of pairs of ^{31}P donors from devices fabricated by the implantation of multiple ions in natural silicon (Dehollain *et al* 2014). The technique has also been applied to implant Er ions into nanoscale field effect transistors in which the optical excitation of the implanted Er ion could be read out electrically (Yin *et al* 2013). The next step for the Si : P devices is the application of deterministic implantation to fabricate large-scale arrays of more than two donor atoms which is the topic of the remainder of this paper.

2. Deterministic implantation

There are two challenges for the fabrication of large-scale arrays by ion implantation. The first is the generation of an implantation signal from the substrate and the second is the positioning of the ion in the desired location. The first challenge can be avoided by trapping single ions in a specially configured ion source which provides one ion at a time to the implanter (Jacob *et al* 2014). However we employ the signal generated by the induction of charge on surface detector electrodes following the dissipation of kinetic energy by ionization after ion impact (Jamieson *et al* 2005). This method allows the counting of ion impacts provided the signal is above the noise threshold of the detector structure which is presently about 1.5 keV. Table 1 shows the requirements for the detection of ionization in the form of electron–hole pairs for various combinations of ions and substrate. In the case of Si : P, the mean pulse for 14 keV ^{31}P has an energy equivalent of about 3.5 keV (see also the discussion below) which allows for high confidence ion counting. However it is desirable to improve the signal-to-noise ratio of this method and also to reduce the implant energy to bring the donors closer to the surface. This has two benefits: reduction of the straggling position uncertainty and improvement of the selectivity of surface electrodes for coupling to specific donors. Simulations based on SRIM 2013.00 (Ziegler *et al* 2010) shown in figure 1 and more detailed considerations (van Donkelaar *et al* 2010) provide an indication of the differences between 14 and 7 keV ^{31}P ions implanted into silicon. The development of a sub-14 keV ^{31}P detection system requires modification of our existing p–i–n on-chip detector electrodes and this is discussed further below.

To address the second challenge of positioning, two approaches have been developed: one based on focused beams using secondary electron emission as the implant signal and the other on surface masks or nanostencils using ion induced charge in the substrate as discussed here. The former method has been used to implant counted 60 keV P (Shinada *et al* 2005), Si (Shinada *et al* 2008) and As (Prati *et al* 2012) ions with an aiming precision around 60 nm. For our applications we ultimately require sub-10 keV ions and 20 nm aiming precision which can potentially be achieved with a small ion implantation system in tandem with a stepped nanostencil. We have developed a scanned nanostencil that acts as a repositionable implantation mask adapted from the technique demonstrated by Schenkel *et al* (Persaud *et al* 2005, Meijer *et al* 2008). A schematic of our system is shown in figure 2. This system can be employed in conjunction with our deterministic implantation scheme to fabricate viable devices supported by theoretical models (Wellard *et al* 2003, van Donkelaar *et al* 2010). Here we illustrate the operation of our system to produce a non-Poisson distribution of implanted ions. For these experiments we employed a stepped nanostencil as a movable mask in conjunction with on-chip detector electrodes that comprise an active substrate to register ion impacts and step the stencil. The active substrate registers single ion impacts from the transient charge pulse of electron–hole pairs induced in the substrate by the stopping of the ion.

The nanostencil developed for the prototype system is shown in figure 3. This stencil was machined in a Si_3N_4 membrane 200 nm thick by a focused ion beam then partially backfilled with Pt dissociated from a precursor gas using a scanning electron beam that also allowed the diameter of the stencil to be monitored in real time. The internal structure of our nanostencils was measured with the scattering of high energy ions (Alves *et al* 2013) and we conclude that miss-strikes in the substrate caused by straggling within the aperture itself will not limit the ability to build workable devices.

The nanostencil was mounted on an attocube stack and scanned over a cooled substrate (120 K) with integrated

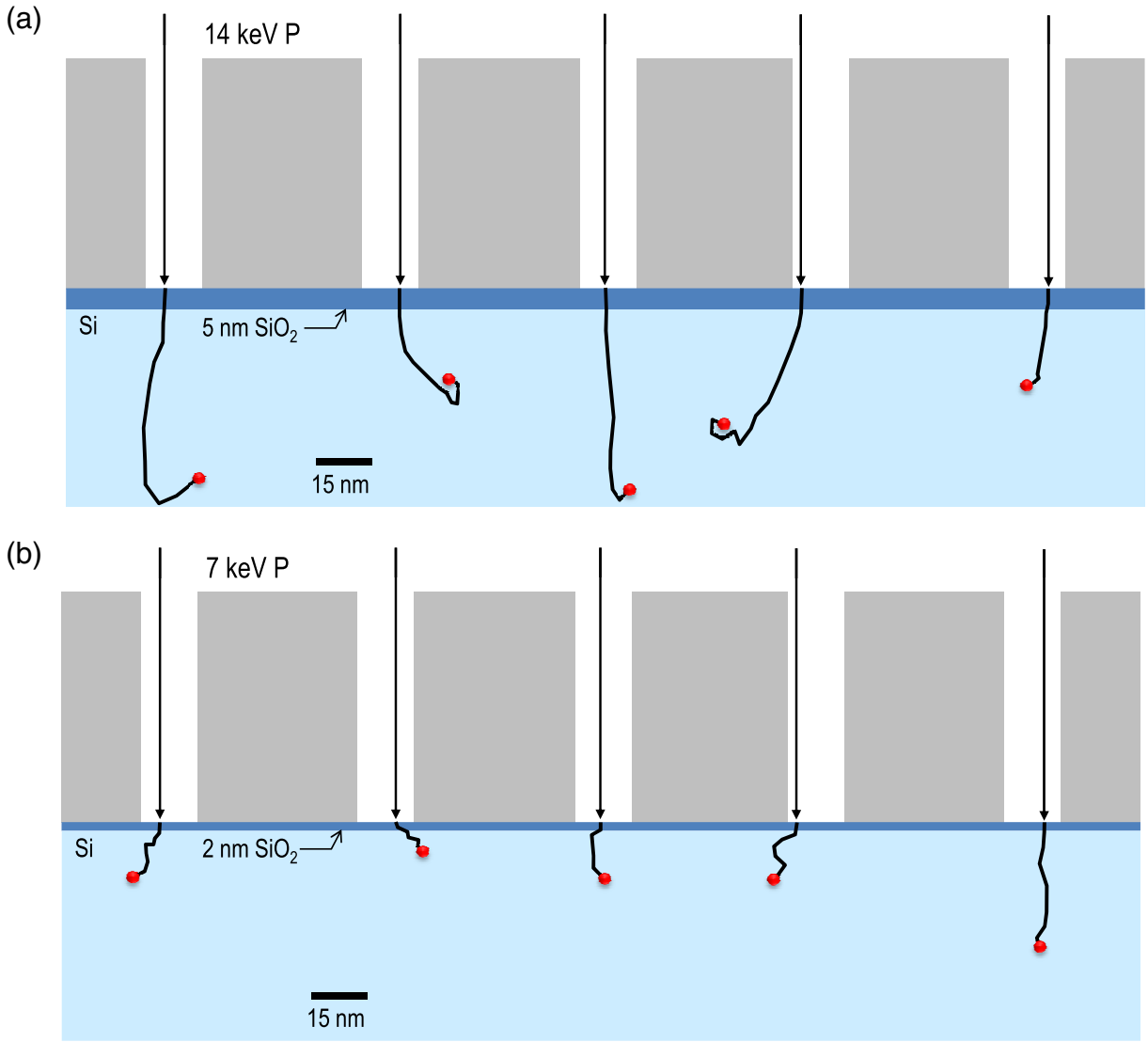

Figure 1. Simulations based on SRIM of the straggling of 14 and 7 keV ^{31}P ions in silicon. Pre-fabricated gate oxides of 5 nm and 2 nm respectively are included in the simulations.

on-chip p–i–n detector electrodes and an oxide mask. The oxide mask was a 200 nm field oxide surrounding a 5 nm gate oxide which had an area of 12 × 12 μm^2. A 14 keV Ar beam was employed for convenience to demonstrate the operation of the system. A discriminator on the pulse height signal from the on-chip detector excluded noise signals below 1.5 keV. The site targeted by the nanostencil was advanced after 0.5 s if no ion impact signals are detected. This was necessary because no signals are detected from the field oxide regions because the range of the ions is insufficient to reach the buried silicon and therefore no signals are expected. The other parameters of the system were nanostencil collimator diameter 80 nm, step size 250 nm, beam 13.5 keV Ar at nominally 4.5 ions s^{-1}. The stage has the capability of a positioning resolution of 0.2 nm over a 12 μm range and a coarse range of 5 mm. We applied this system to implant 100 × 100 sites across a 25 × 25 micrometre square region of our substrate. In this test only the central approximately 40 × 40 sites were located within the thin oxide region which is sensitive to ions entering the substrate.

With regard to the signals from the sites in the thin oxide region, a histogram of the number of impacts per site is shown in figure 4. This histogram is compared to a Poisson distribution for a mean of six signals. The measured results show, as expected, a non-Poisson distribution imposed by the ion detection system. The histogram shows about two-thirds of the sites received less than 6 counts because of non-systematic variations in the current from our implanter when collimated to the low beam current necessary to minimize pulse pile-up. The incident ion fluence varied from a full current mode to a reduced current mode that caused the interval between ion impacts to exceed the 0.5 s limit set by the stepping system whereupon the nanostencil advanced to the next site. Appropriate tuning of the system parameters can overcome this issue.

With regard to the signals registered from the thick field oxide region where the ions could not reach the substrate, there were 1350 sites located in the thick field oxide region and these sites contributed only 25 false-positive signals (1.4%) from 25 sites that produced one signal. These signals almost

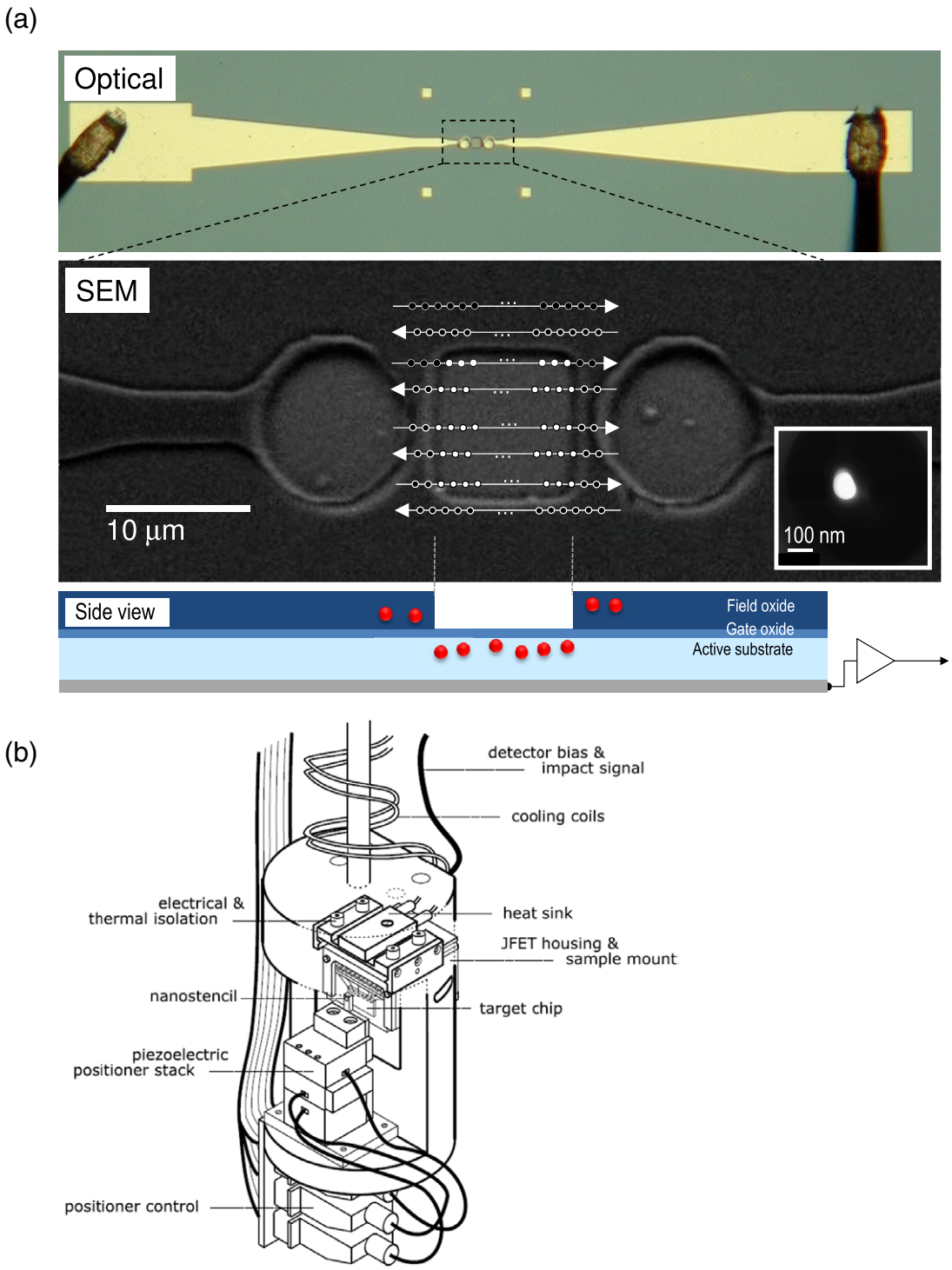

Figure 2. (*a*) The step and repeat deterministic implantation of a large-scale single atom array with a stepped nanostencil gated on ion impact signals from the substrate. The white dots represent the impact sites (not to scale) over the thin oxide region where ions can enter the substrate. The open dots represent sites over the thick field oxide where ions cannot enter the substrate. (*b*) The experimental scanned nanostencil apparatus used for the present experiments.

certainly arise from straggling in the collimator causing ions to diverge and impact in the thin oxide region even though the collimator in the nanostencil was located over the thick field oxide region. Our model for these events for an experimental configuration similar to the present experiments suggests the false-positive signal rate should be around 0.7% (Alves *et al* 2013) which is consistent with our finding. Our present system is very sensitive to such scattering because we were obliged to position the nanostencil more than 700 μm above the substrate to clear the wire bonds to the detector electrodes. This can be reduced in an optimized system. Also, the use of an appropriate surface mask over the thin oxide region can greatly reduce this background. To develop this system further requires foreseeable reductions in the diameter of the nanostencil and

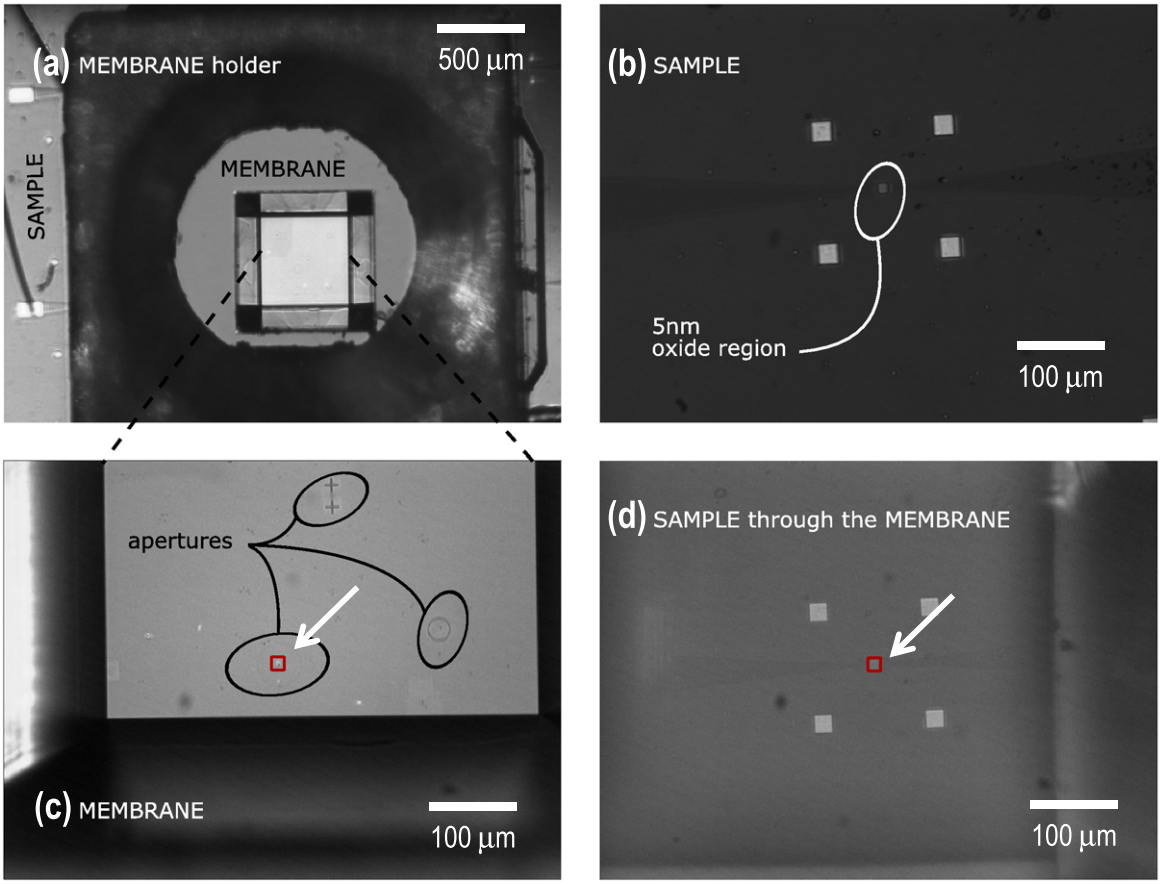

Figure 3. Optical micrographs of various scales showing the nanostencil used in the present experiments. The sample to be implanted is visible through the semi-transparent stencil fabricated in a Si_3N_4 membrane. (*a*) View along direction of ion incidence showing the membrane in which the nanostencil has been fabricated with the sample to be implanted behind. Wire bonds to the on-chip detector electrodes are visible to the left. (*b*) The central region of the sample showing four alignment markers surrounding the thin oxide region. (*c*) Close-up of the apertures machined in the membrane acting as the nanostencil. The aperture used to collimate the beam for the present experiments is arrowed. (*d*) Same view as (*b*) but with the partially transparent membrane in place.

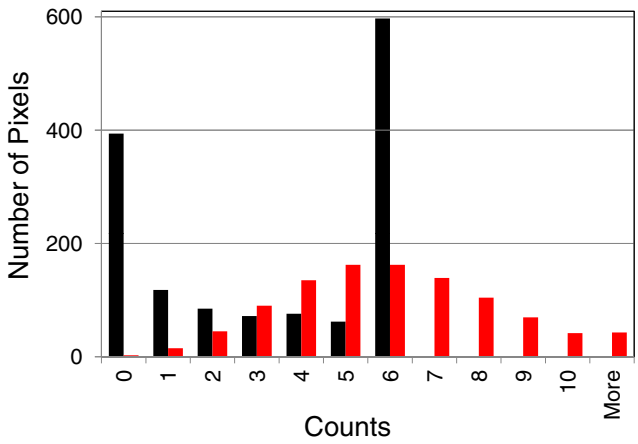

Figure 4. Experimental histogram of the number of ions per site employing signals from the on-chip detector electrodes for the configuration shown in figure 2(*a*). See text for a discussion of the gating protocol and the sites that received fewer than six ions. The coloured bars represent the normalised Poisson distribution for a peak of six ions.

we have already demonstrated a diameter of 30 nm (Alves *et al* 2013). Also required is a reduction in the beam energy as discussed to reduce straggling. We now turn to the progress towards this latter goal.

3. On-chip detection system

Although the electron–hole pairs induced by ion impact produce a high signal-to-noise ratio signal in our p–i–n on-chip detector electrodes, this advantage reduces for sub-10 keV ions owing to the encroachment of noise. Two developments are possible to address this issue. Both require modification of the detector structure to produce internal charge gain from electron avalanches triggered in the substrate by high electric fields. At moderate fields the avalanche process is self-quenched and the signals are linearly proportional to the ionization. At high fields the device is operated in Geiger mode and the avalanche process is not self-quenched. In this case the device therefore requires a transient bias pulse, synchronized with a beam gate, to ready the device to receive an ion then quench the avalanche if an ion impact occurs. In principle a single electron–hole pair can trigger the Geiger mode avalanche which represents the ultimate sensitivity. Both modes of operation are in routine application in silicon devices to detect incident photons with high sensitivity (Akiba *et al* 2005, Campbell 2007, Ghioni *et al* 2007, Tsujino *et al* 2007) including several quantum key distribution experiments (Hughes 2002, Kurtsiefer 2002, Poppe 2004, Schmitt-Manderbach 2007, Pelso 2009).

Modifying our existing p–i–n detector design to incorporate the higher electric field that triggers ion-impact-induced avalanches, in conjunction with thinner gate oxides, provides an effective solution for implanting low energy ions (sub-10 keV) (Seamons *et al* 2008, Bielejec *et al* 2010, Yang and Jamieson 2010) and reduced ion implantation straggling uncertainty. In the case of the Si : P system, our previous generation of p–i–n detectors provided a typical detection limit about 1.5 keV for the measurement of 3.5 keV ionization energy arising from single 14 keV P ion implants in the silicon substrate (Jamieson *et al* 2005) through a pre-fabricated 5 nm SiO_2 surface gate oxide. The ionization energy in this context is the energy equivalent to the number of electron–hole pairs detected by the device which is governed by the energy required to create an electron–hole pair in silicon and the proportion of the initial ion kinetic energy that contributes to ionization. Under these conditions the ion placement accuracy is limited by ion straggling to about 8 nm for P ions implanted 20 nm deep (table 1). This can be reduced below 8 nm with a sub-10 keV P ion but this produces much less ionization energy, near the detection limit of a p–i–n detector. Use of heavier donors than P has the advantage of higher precision (Naganawa *et al* 2008) and more induced charge (table 1) which will be useful in some applications. However we seek to exploit the spin-half ^{31}P nucleus and the heavier donors do not have this attribute. For sub-10 keV P ions, the development of a modified p–i–n structure in which ion-impact-induced avalanches occur leads to internal charge gain which overcomes the problem of low induced charge. Further, we have already done realistic simulations and have shown the yield of useful devices for sub-10 keV P implants is reasonable (van Donkelaar *et al* 2010) hence the effort is justified.

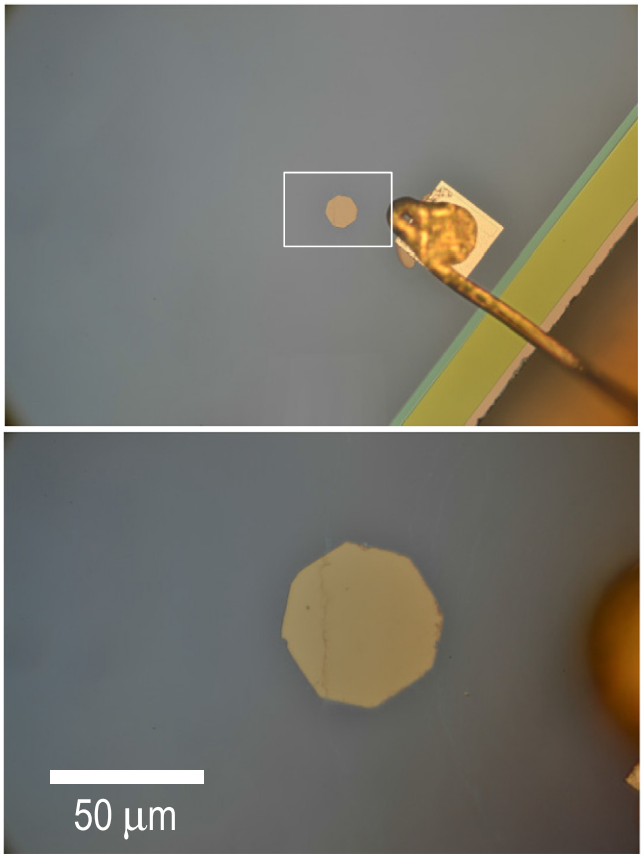

Figure 5. Optical micrograph of the region of the modified avalanche photodiode device similar to the one used in the present experiments where the surface layer has been etched away to expose the silicon substrate. The scale is given by the width of the etched region which is nominally 50 μm.

4. Experiment

Although the response of avalanche photo diodes has been examined with high energy light ions (∼MeV) it has been observed that their response to low energy heavy ions (sub-15 keV) has not been extensively investigated to date (Ogasawara *et al* 2012). This is possibly because the devices that are readily available are configured with a thick surface dead layer that does not allow the low energy heavy ions to enter the active region of the device. For our experiments, we modified a commercial device by thinning the dead layer and employed the modified device to obtain an energy pulse height spectrum to examine the response to 14 keV ^{31}P ions. We employed a Hamamatsu type S5343 APD device, active area 0.78 mm^2, which was selected because the internal high electric field that induces avalanches is on the back of the device opposite to the normal photon incidence surface and this produces higher charge gain in our application. In addition these devices have a relatively small capacitance and low dark current which minimizes noise. The device was modified by etching away the surface passivation layer over a nominal 50 × 50 μm^2 window to expose the surface of the silicon. A micrograph of a quantum device subject to this process is shown in figure 5. This window allows our low energy heavy ions to enter the active region of the device which would otherwise be stopped in the intact surface dead layer. The electrical characteristics of the device were not affected by this process.

The modified device was then loaded into our ion implantation system and connected to our electronics chain (Jamieson *et al* 2005) and multichannel analyser to record the ionization energy pulse height spectrum. The vacuum in the system was maintained at 10^{-7} Torr to prevent contamination of the surface of the device which would otherwise prevent ions entering the substrate. The device was cooled to further minimize the dark current signals.

The experimental pulse height spectrum from a representative modified device exposed to 14 keV ^{31}P ions in shown in figure 6. Two spectra are shown: the first for relatively low reverse bias (−20 V) potential where no avalanches occur and the second for higher bias potential (−135 V) sufficient to induce avalanches. The higher bias potential was selected to maintain a linear gain of ∼3.1 which was sufficient to separate the ion impact signal from the noise threshold. The energy spectrum for the low bias is as expected from our previous work (Jamieson *et al* 2005) and the peak observed for the high bias is very similar but shifted to higher effective energy owing to the internal charge gain.

We have compared our experimental energy spectra to simulations from SRIM using the following process. SRIM

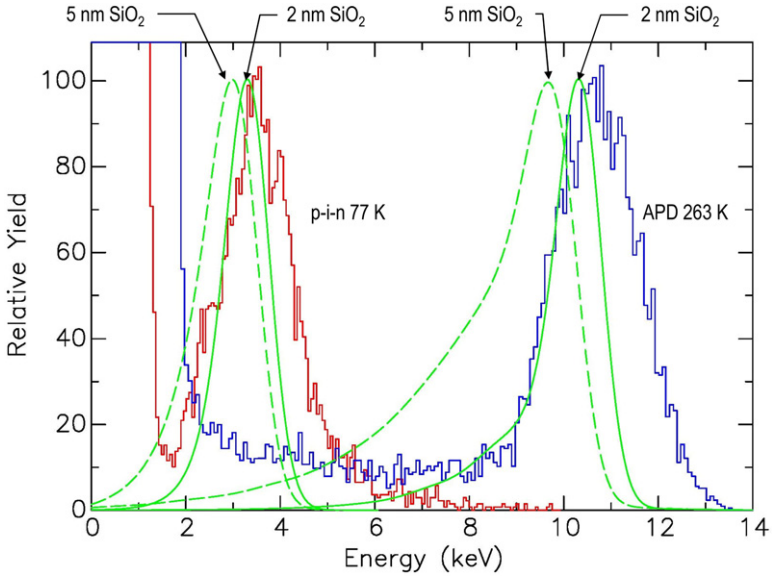

Figure 6. Experimental pulse height spectra as a function of ionization energy for 14 keV P ions incident on our modified avalanche photodiode device operated with (i) a relatively low bias potential so that ion-impact-induced avalanches do not occur (red histogram, peak at 3.5 keV) and (ii) a relatively high bias so that ion-impact-avalanches occur with an internal charge gain of ∼3.1 (blue histogram, peak at ∼11 keV). The temperature of the device was 77 K for low bias and 263 K for high bias to reduce thermal noise. Superimposed on the experimental spectra are simulations discussed in the text (green smooth and broken curves for 2 nm and 5 nm surface SiO_2 dead layer respectively).

was used to simulate the passage of many ions through a thin surface oxide. To examine the effect of the oxide, 2 and 5 nm thick SiO_2 surface layers were modelled and the energy distribution of each transmitted ion was obtained. We included both the primary ions (P) and the forward recoils from the oxide (O, Si). This distribution was then scaled by the appropriate factor experimentally obtained by Funsten *et al* (2004) for ion irradiation of silicon detectors that represents the share of the ion kinetic energy leading to ionization in the Si matrix. The simulation at this point suggests a small proportion of ions produce no ionization. For example this is 0.1% for 14 keV ^{31}P ions incident through a 5 nm SiO_2 surface layer and 0.01% for 14 keV ^{31}P ions incident through a 2 nm SiO_2 surface layer. These proportions represent a limit to the precision of our method. Next we convolved the ionization energy distribution with the experimental energy resolution which was given approximately by the FWHM of the noise peaks in the experimental spectra. We used a FWHM of 1 keV which was similar to the values for the experimental spectra of 0.8 and 1.1 keV for low and high bias respectively. To simulate the avalanche process the simulated ionization energy spectrum was multiplied by the experimental charge gain of 3.1 before convolution with the energy resolution. These simulations do not account for the effect of variations in the ionization arising from the statistics of the stopping process which will broaden the energy peaks further. The resulting simulations are shown in figure 6.

Comparing these simulations to the observed energy spectra reveals some differences. First the simulated peaks, regardless of dead layer thickness, have a lower energy than experiment. This suggests that the energy loss in the actual surface dead layer was less than that for 2 nm of SiO_2. This is possible because the etching process was devised to selectively remove all the surface oxide comprising the dead layer and the device was placed under vacuum immediately after the etch was completed to minimize the formation of a native oxide on the exposed silicon. Also, the width of the simulated peaks are generally narrower then experiment which is due to the omission of the statistical variations in the ionization from the model. However the simulation for the 5 nm oxide high bias peak has a long low energy tail which has a higher amplitude than that seen in the experiment. This tail arises from the straggling of the ions in the 5 nm thick oxide which, as we have observed, is not likely present in the actual device. The experimental high bias peak has a low energy tail which extends to lower energy than the simulation. It is most likely this tail arises from ion impacts into the unetched regions of the device where some straggling of forward recoils can occur, or where the avalanche process is incomplete owing to fringe fields at the edge of the device (Ogasawara *et al* 2012), but these effects were not modelled. It is also possible the differences between the experimental protocol of Funsten *et al* (2004) leads to a different energy spectrum compared to our situation which would invalidate the model. The main difference is that the former employed a dc amplifier to measure both a continuous beam current of ions and an induced ionization charge current with all the contributions from both fast and slow components of charge transport in the device. However we employed a band-pass amplifier to record a single ion induced charge pulse which had only the contribution from the fast charge transport component. However our numerical simulations for charge drift in a pristine p–i–n device suggest the ion-impact-induced transient signal should be of duration no longer than 0.5 μs (Jamieson *et al* 2005), well within the time span of our system.

5. Conclusion

We have demonstrated a system for the implantation of non-Poisson distributions of heavy ions in a silicon substrate based on a stepped nanostencil gated on signals from the substrate from on-chip detector electrodes. Foreseeable improvements in the spatial resolution which include the use of a smaller collimator in the nanostencil and more sensitive on-chip detector electrodes will allow higher precision arrays to be constructed from sub-10 keV ions. As the first step, we demonstrated that we could exploit the internal charge gain of a modified commercially available Si APD device to measure the ionisation produced by sub-15 keV P heavy ion impacts. We have investigated the modification of the architecture of our on-chip detector electrodes reported previously (Jamieson *et al* 2005) and conclude that incorporation of a heavily doped back layer will allow reliable signals to be obtained for sub-10 keV P implants into undoped surface regions of the chip to construct deterministic arrays of donors. This will be required for improved spatial and depth precision of the deterministic implantation process.

Acknowledgments

This research was conducted by the Australian Research Council Centre of Excellence for Quantum Computation and Communication Technology (project number CE110001027) and the US Army Research Office (grant number W911NF-08-1-0527). We acknowledge useful discussions with Thomas Schenkel, Kilian Singer and Jan Meijer. We thank Kumar Ganesan for performing the etching of the modified detectors.

References

Akiba M, Fujiwara M and Sasaki M 2005 Ultrahigh-sensitivity high-linearity photodetection system using a low-gain avalanche photodiode with an ultralow-noise readout circuit *Opt. Lett.* **30** 123

Alves A D C, Newnham J, van Donkelaar J A, Rubanov S, McCallum J C and Jamieson D N 2013 Controlled deterministic implantation by nanostencil lithography at the limit of ion-aperture straggling *Nanotechnology* **24** 145304

Batra A, Weis C D, Reijonen J, Persaud A, Schenkel T, Cabrini S, Lo C C and Bokor J 2007 Detection of low energy single ion impacts in micron scale transistors at room temperature *Appl. Phys. Lett.* **91** 193502

Bielejec E, Seamons J A and Carroll M S 2010 Single ion implantation for single donor devices using Geiger mode detectors *Nanotechnology* **21** 085201

Campbell J C 2007 Recent advances in telecommunications avalanche photodiodes *J. Light Wave Technol.* **25** 109

Chason E *et al* 1997 Ion beams in silicon processing and characterization *J. Appl. Phys.* **81** 6513

Dehollain J P, Muhonen J T, Tan K Y, Saraiva A, Jamieson D N, Dzurak A S and Morello A 2014 Single-shot readout and relaxation of singlet and triplet states in exchange-coupled P-31 electron spins in silicon *Phys. Rev. Lett.* **112** 236801

Dowling J P and Milburn G J 2003 Quantum technology: the second quantum revolution *Phil. Trans. R. Soc. Lond.* A **361** 1655–74

Funsten H O, Ritzau S M, Harper R W, Borovsky J E and Johnson R E 2004 Energy loss by keV ions in silicon *Phys. Rev. Lett.* **92** 213201

Gibbons J F 1987 Historical perspectives on ion implantation *Nucl. Instrum. Methods* **B21** 83–9

Ghioni M, Gulinatti A, Rech I, Zappa F and Cova S 2007 Progress in silicon single-photon avalanche diodes *IEEE J. Sel. Top. Quantum Electron.* **13** 852

Hughes R J, Nordholt J E, Derkacs D and Peterson C G 2002 Practical free-space quantum key distribution over 10 km in daylight and at night *New J. Phys.* **4** 43

Jacob G, Groot-Berning K, Wolf S, Ulm S, Couturier L, Poschinger U G, Schmidt-Kaler F and Singer K 2014 Single particle microscopy with nanometer resolution (arXiv:1405.6480v1)

Jamieson D N, Prawer S, Andrienko I, Brett D A and Millar V 2001 A role for ion implantation in quantum computing *Nucl. Instrum. Methods Phys. Res.* B **175-177** 744–50

Jamieson D N *et al* 2005 Controlled shallow single-ion implantation in silicon using an active substrate for sub-20-keV ions *Appl. Phys. Lett.* **86** 202101

Johnson B C *et al* 2010 Drain current modulation in a nanoscale field-effect-transistor channel by single dopant implantation *Appl. Phys. Lett.* **96** 264102

Koiller B, Hu X D and Das Sarma S 2006 Electric-field driven donor-based charge qubits in semiconductors *Phys. Rev.* B **73** 045319

Kurtsiefer C, Zarda P, Halder M, Weinfurter H, Gorman P M, Tapster P R and Rarity J G 2002 A step towards global key distribution *Nature* **419** 450

Laucht A, Kalra R, Muhonen J T, Dehollain J P, Mohiyaddin F A, Hudson F, McCallum J C, Jamieson D N, Dzurak A S and Morello A 2014 High-fidelity adiabatic inversion of a P-31 electron spin qubit in natural silicon *Appl. Phys. Lett.* **104** 92115

Meijer J *et al* 2008 Towards the implanting of ions and positioning of nanoparticles with nm spatial resolution *Appl. Phys.* A **91** 567–71

Morello A *et al* 2010 Single-shot readout of an electron spin in silicon *Nature* **467** 687–91

Muhonen J T, Dehollain J P, Laucht A, Hudson F E, Kalra R, Sekiguchi T, Itoh K M, Jamieson D N, McCallum J C, Dzurak A S and Morello A 2014 Storing quantum information for 30 seconds in a nanoelectronic device *Nature Nanotechnol.* **9** 986–91

Naganawa M, Kawamura Y, Shimizu Y, Uematsu M, Itoh K M, Ito H, Nakamura M, Ishikawa H and Ohji Y 2008 Accurate determination of the intrinsic diffusivities of boron, phosphorus, and arsenic in silicon: the influence of SiO_2 films *Japan. J. Appl. Phys.* **47** 6205

Naydenov B, Reinhard F, Lämmle A, Richter V, Kalish R, D'Haenens-Johansson U F S, Newton M, Jelezko F and Wrachtrup J 2010 Increasing the coherence time of single electron spins in diamond by high temperature annealing *Appl. Phys. Lett.* **97** 242511

Ogasawara K, Allegrini F, Desai M I, Livi S and McComas D J 2012 A linear mode avalanche photodiode for ion detection in the energy range 5–250 keV *IEEE Trans. Nucl. Sci.* **59** 2601–7

Persaud A, Park S J, Liddle J A, Schenkel T, Bokor J and Rangelow I W 2005 Integration of scanning probes and ion beams *Nano Lett.* **5** 1087–91

Pelso M P, Gerhardt I, Ho C, Lamas-Linares A and Kurtsiefer C 2009 Daylight operation of a free space, entanglement-based quantum key distribution system *New J. Phys.* **11** 045007

Pla J J, Tan K Y, Dehollain J P, Lim W H, Morton J J L, Jamieson D N, Dzurak A S and Morello A 2012 A single-atom electron spin qubit in silicon *Nature* **489** 541–5

Pla J J, Tan K Y, Dehollain J P, Lim W H, Morton J J L, Zwanenburg F A, Jamieson D N, Dzurak A S and Morello A

2013 High-fidelity readout and control of a nuclear spin qubit in silicon *Nature* **496** 334–8
Poate J M and Saadatmand K 2002 Ion beam technologies in the semiconductor world *Rev. Sci. Instrum.* **73** 868
Poppe A *et al* 2004 Practical quantum key distribution with polarization entangled photons *Opt. Express* **12** 3865
Prati E, Hori M, Guagliardo F, Ferrari G and Shinada T 2012 Anderson–Mott transition in arrays of a few dopant atoms in a silicon transistor *Nature Nanotechnol.* **7** 443–7
Rose P H 1985 A history of commercial implantation *Nucl. Instrum. Methods* **B6** 1–8
Schofield S R, Curson N J, Simmons M Y, Rueß F J, Hallam T, Oberbeck L and Clark R G 2003 Atomically precise placement of single dopants in Si *Phys. Rev. Lett.* **91** 136104
Schwartz J, Michaelides P, Weis C D and Schenkel T 2011 *In situ* optimisation of co-implantation and substrate temperature conditions for nitrogen-vacancy centre formation in single-crystal diamonds *New J. Phys.* **13** 035022
Schmitt-Manderbach T *et al* 2007 Experimental demonstration of free-space decoy-state quantum key distribution over 144 km *Phys. Rev. Lett.* **98** 010504
Seamons J A, Bielejec E, Carroll M S and Childs K D 2008 Room temperature single ion detection with Geiger mode avalanche diode detectors *Appl. Phys. Lett.* **93** 043124
Shinada T, Kurosawa T, Nakayama H, Zhu Y, Hori M and Ohdomari I 2008 A reliable method for the counting and control of single ions for single-dopant controlled devices *Nanotechnology* **19** 345202
Shinada T, Okamoto S, Kobayashi T and Ohdomari I 2005 Enhancing semiconductor device performance using, ordered dopant arrays *Nature* **437** 1128–31
Toyli D M, Weis C D, Fuchs G D, Schenkel T and Awschalom D D 2010 Chip-scale nanofabrication of single spins and spin arrays in diamond *Nano Lett.* **10** 3168–72
Tsujino K, Akiba M and Sasaki M 2007 Ultralow-noise readout circuit with an avalanche photodiode: toward a photon-number-resolving detector *Appl. Opt.* **46** 1009
van Donkelaar J A, Greentree A D, Alves A D C, Jong L M, Hollenberg L C L and Jamieson D N 2010 Top-down pathways to devices with few and single atoms placed to high precision *New J. Phys.* **12** 065016
Wegmann L 1980 Historical perspectives and future trends for ion implantation systems *Nucl. Instrum. Methods* **189** 1–6
Wellard C J, Hollenberg L C L, Parisoli F, Kettle L M, Goan H S, McIntosh J A L and Jamieson D N 2003 Electron exchange coupling for single donor solid-state spin qubits *Phys. Rev.* B **68** 195209
Yang C Y and Jamieson D N 2010 Investigation of avalanche silicon detectors for low energy single ion implantation applications *Nucl. Instrum. Methods Phys. Res.* **268** 2034–7
Yin C M, Rancic M, deBoo G G, Stavria N, McCallum J C, Sellars M J and Rogge S 2013 Optical addressing of an individual erbium ion in silicon *Nature* **497** 91
Ziegler J F, Ziegler M D and Biersack J P 2010 SRIM—the stopping and range of ions in matter *Nucl. Instrum. Methods Phys. Res.* **268** 1818–23